Supplementary Material

# Flexible 3D continuous GNSs/CNTs tube-network elastomer composites for high-performance EMI shielding and strain sensing

Yang Zhou, Xinjia Yu, Jiaxin Liu, Hu Long, Tielin Shi (✉)

State key Laboratory of Intelligent Manufacturing Equipment and Technology, School of Mechanical Science and Engineering, Huazhong University of Science and Technology, Wuhan 430074, China

**Corresponding author**

Tielin Shi - School of Mechanical Science and Engineering, Huazhong University of Science and Technology, Wuhan 430074, China; Email: tlshi@hust.edu.cn

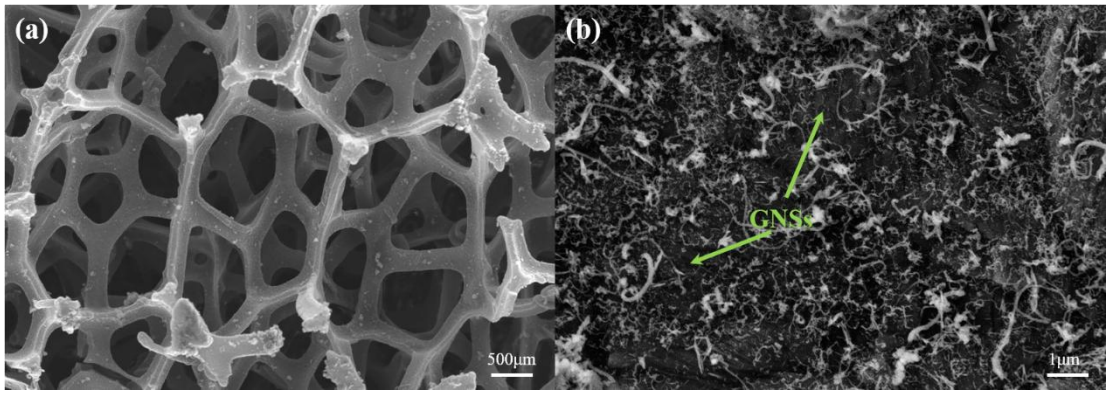


**Fig. S1** SEM images of (a) the nickel foam/tube-network composite grown for 0.5 h and (b) the external surface of the GNSs/CNTs@0.5h tube-network structure.

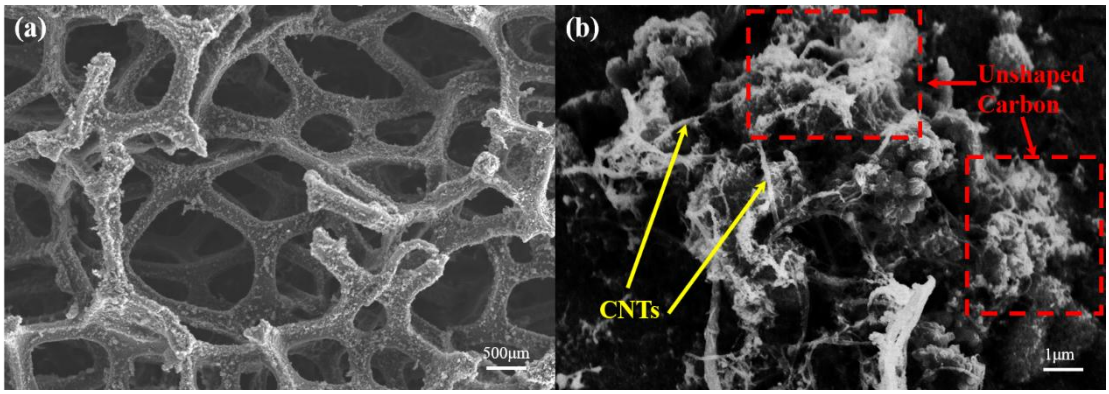


**Fig. S2** SEM images of (a) the nickel foam/tube-network composite grown for 1.5 h and (b) the external surface of the GNSs/CNTs@1.5h tube-network structure.

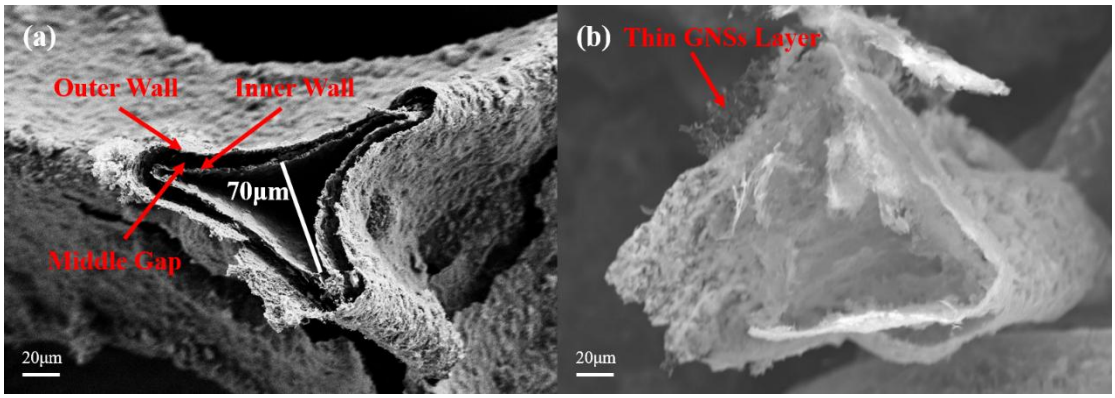


**Fig. S3** SEM images of the fracture surfaces of the GNSs/CNTs tube-network: (a) smooth cleavage surface and (b) irregular fracture surface.

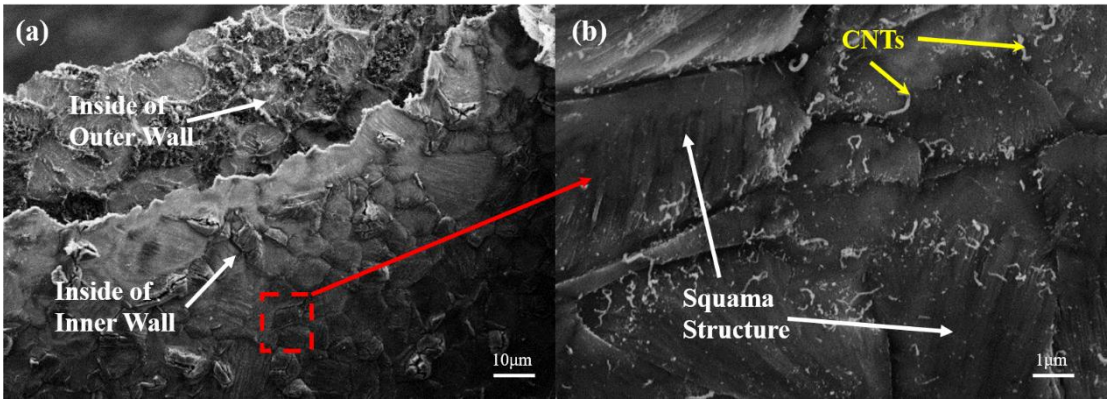


**Fig. S4** SEM images of the internal surface of the GNSs/CNTs@0.5h structure.

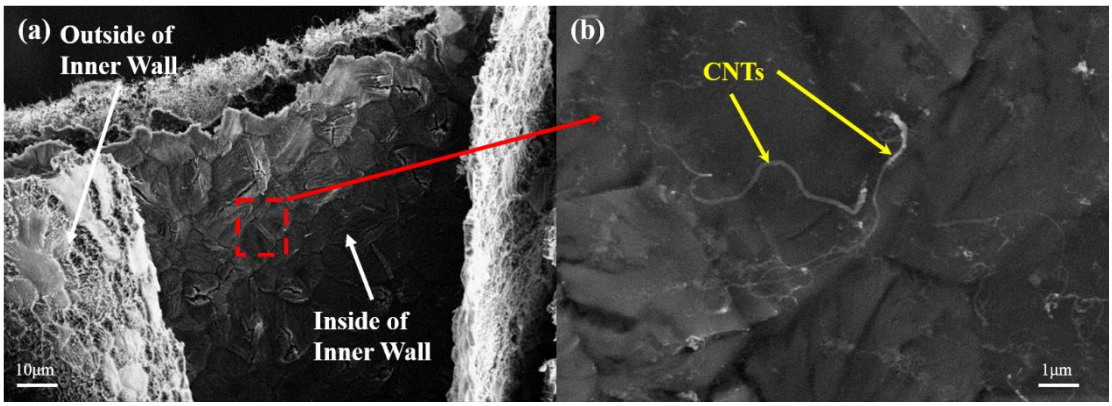


**Fig. S5** SEM images of the internal surface of the GNSs/CNTs@1h structure.

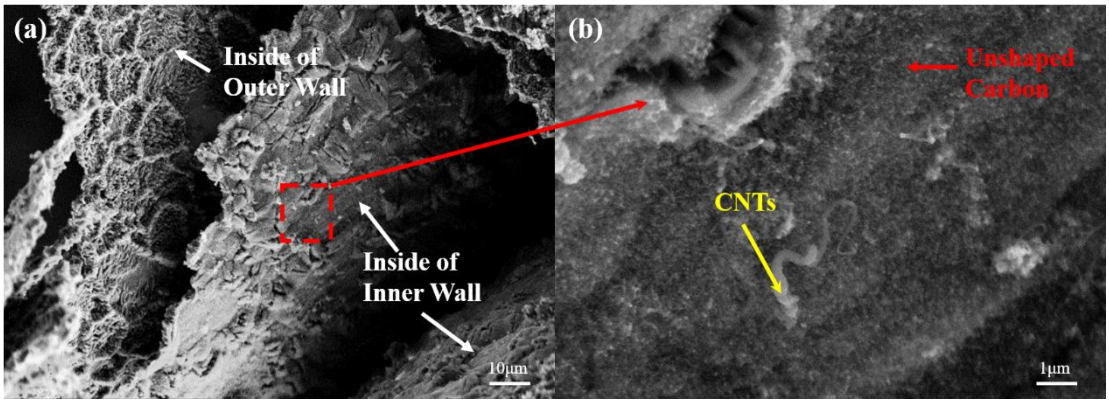


**Fig. S6** SEM images of the internal surface of the GNSs/CNTs@1.5h structure.

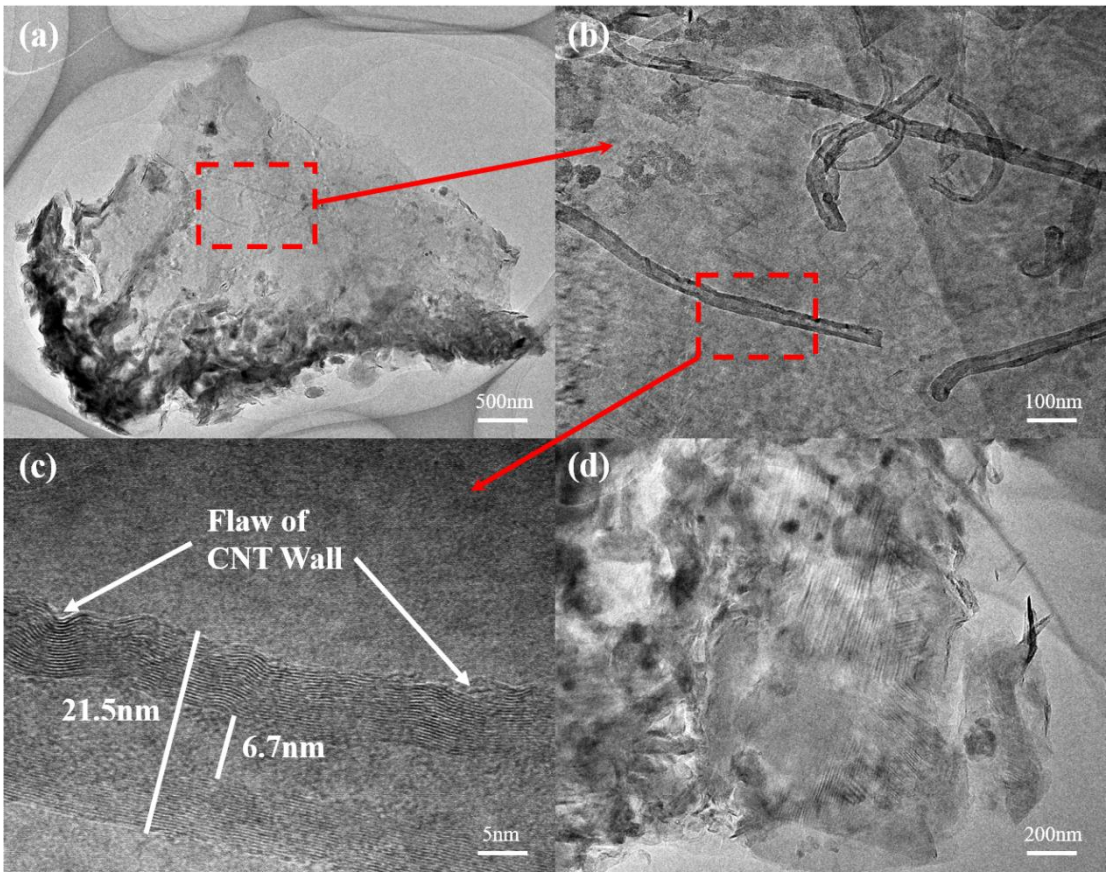


**Fig. S7** TEM images of the GNSs/CNTs@0.5h composite: (a) overview of the GNSs; (b, c) morphology of the CNTs; and (d) high-resolution lattice texture of the GNSs.

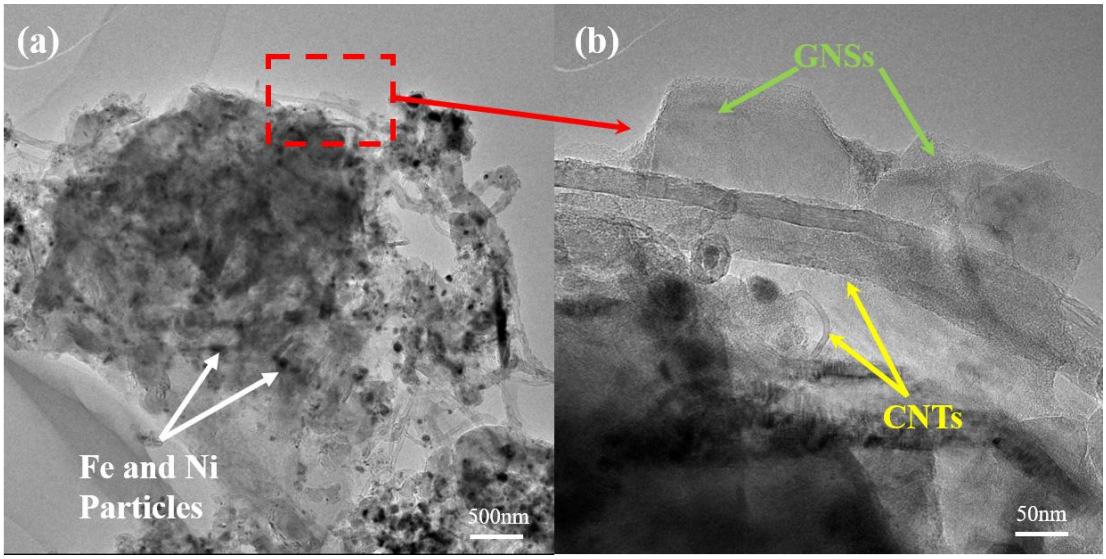


**Fig. S8** TEM images of the GNSs/CNTs@1h composite: (a) overview of the GNSs and (b) morphology of the CNTs.

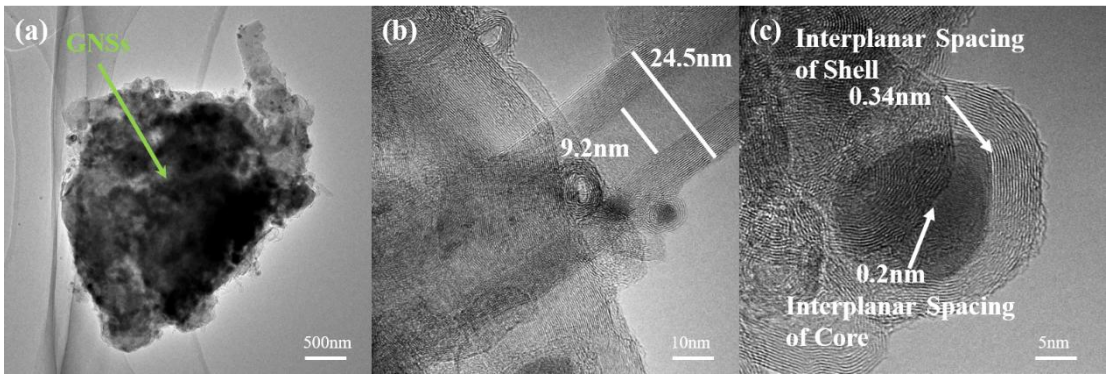


**Fig. S9** TEM images of the GNSs/CNTs@1.5h composite: (a) overview of the GNSs and (b, c) morphology of the CNTs.

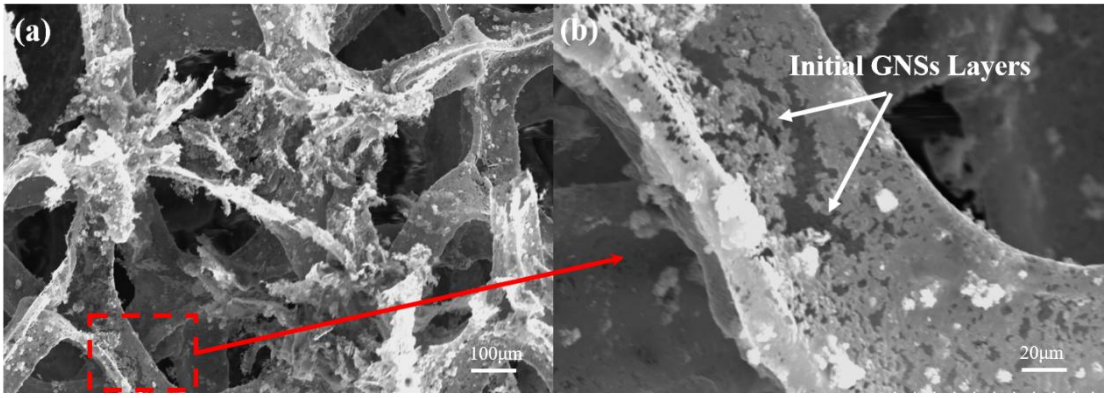


**Fig. S10** SEM images of the GNSs/CNTs structure during the initial growth stage (5 min).

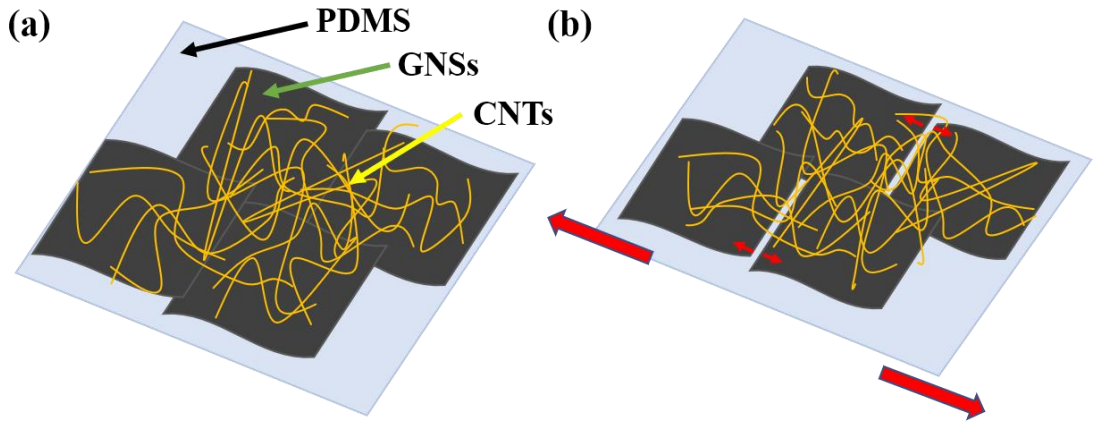


**Fig. S11** Schematic illustration of the microstructural deformation mechanism of the C-PDMS composite: (a) original C-PDMS; (b) stretched C-PDMS.

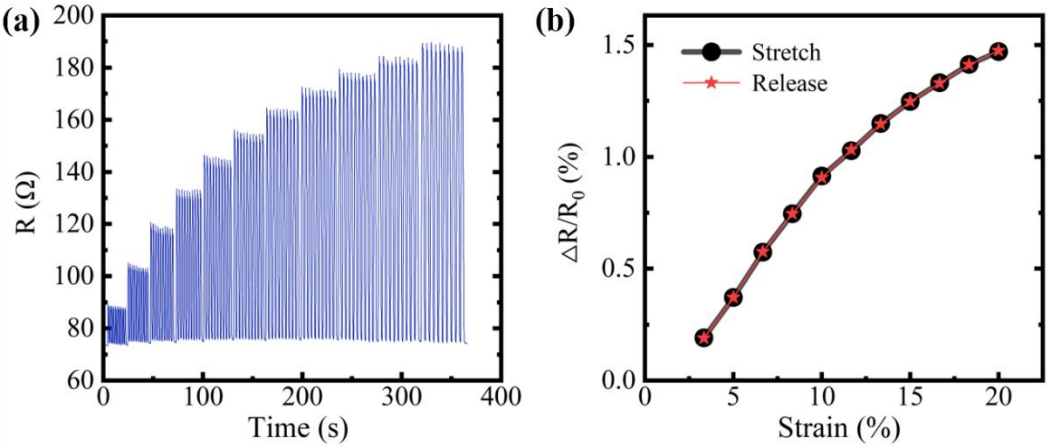


**Fig. S12** Resistance-strain hysteresis curves of the C-PDMS composite during dynamic stretch-release cycles.

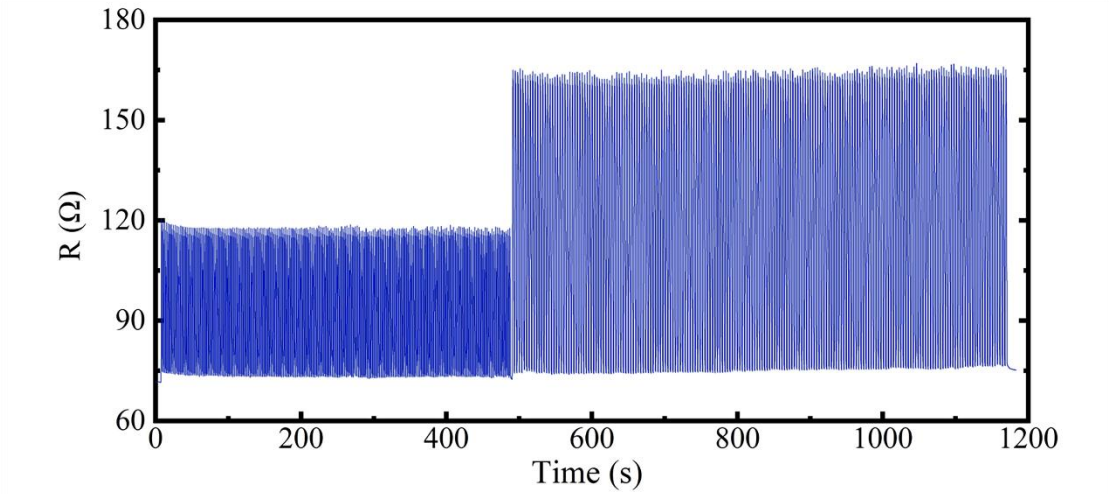


**Fig. S13** Dynamic resistance-strain profiles of the C-PDMS composite during cyclic fatigue testing.

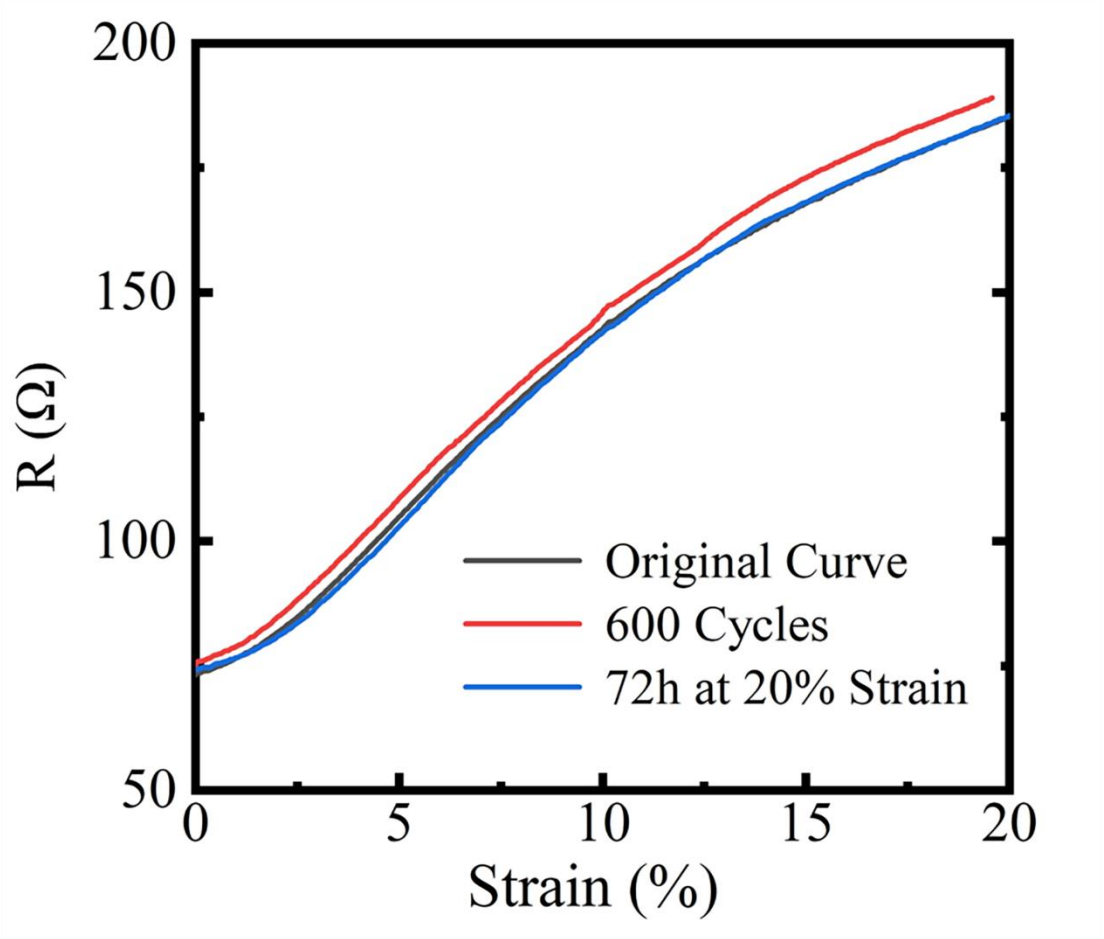


**Fig. S14** Comparison of the resistance-strain curves of the C-PDMS composite before and after extensive fatigue testing.

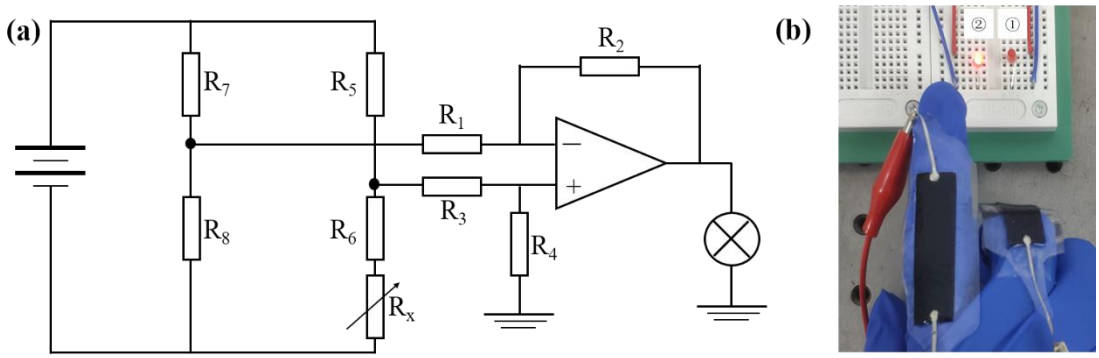


**Fig. S15** A conceptual strain-sensing circuit integrating the C-PDMS sensor and an LED indicator: (a) circuit schematic diagram and (b) optical photographs of the assembled device.

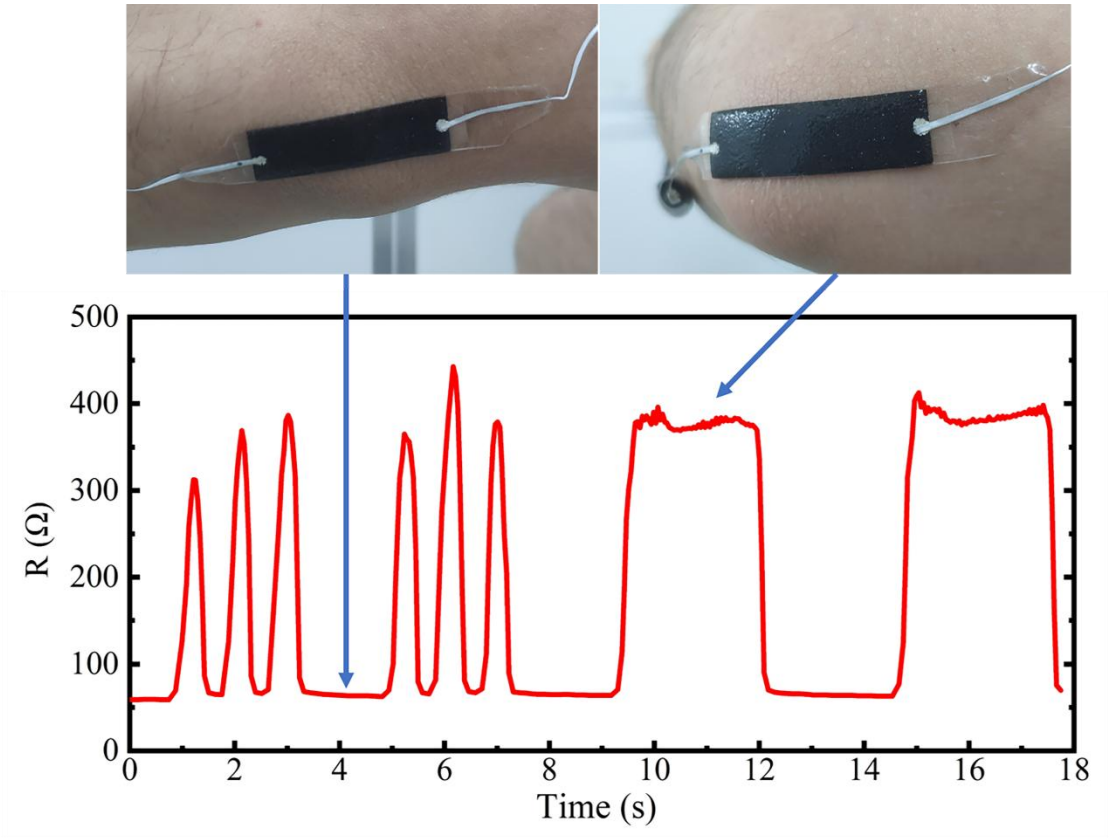


**Fig. S16** Real-time relative resistance variations of the C-PDMS sensor attached to the elbow for monitoring joint flexion.

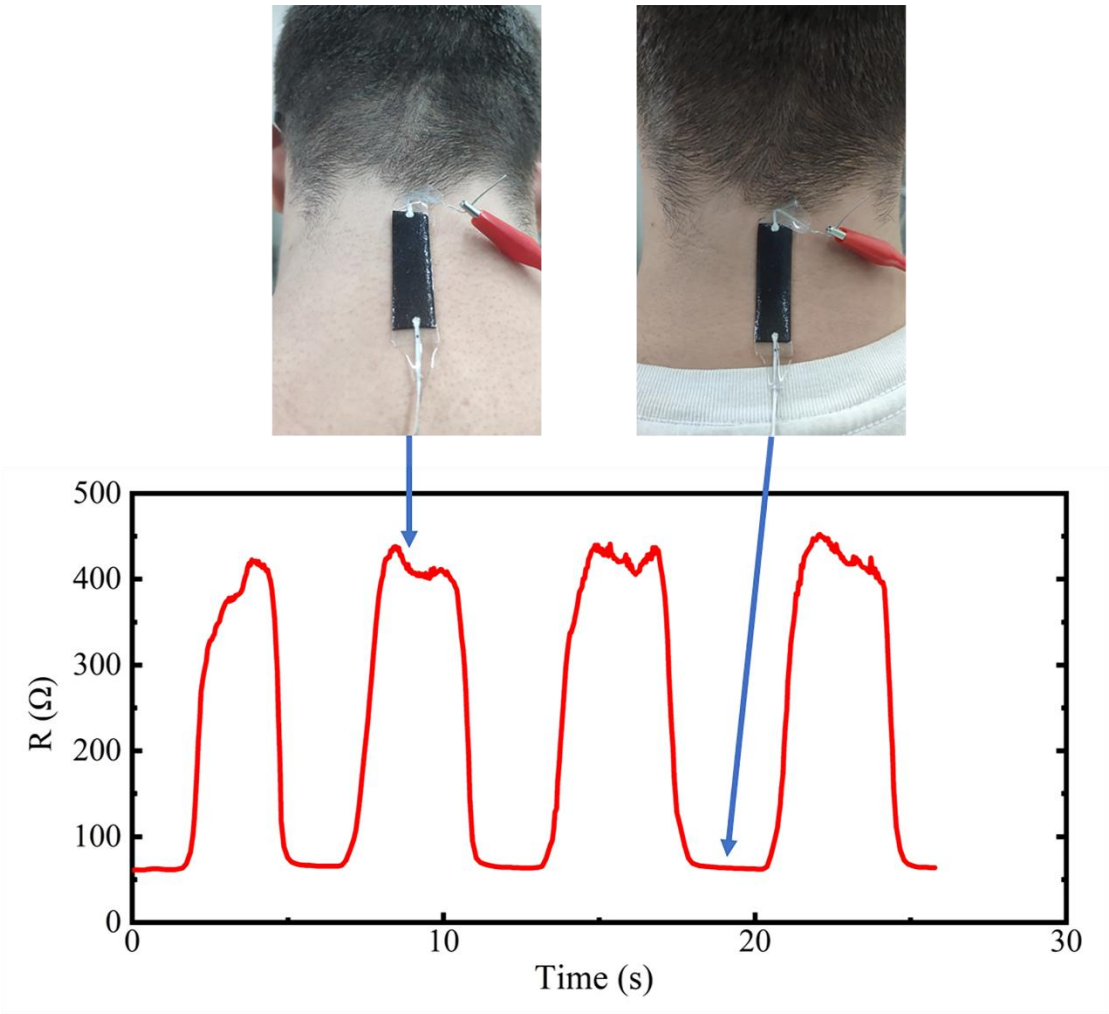


**Fig. S17** Real-time relative resistance variations of the C-PDMS sensor attached to the cervical spine for monitoring neck movements.